Limits to surface-enhanced Raman scattering near arbitrary-shape scatterers

Limits to surface-enhanced Raman scattering near arbitrary-shape scatterers

Benzaouia, Mohammed, Michon, Jérôme, Christiansen, Rasmus, Yao, Wenjie, Miller, Owen, et al.

Mohammed Benzaouia, Jérôme Michon, Rasmus E. Christiansen, Wenjie Yao, Owen D. Miller, Ole Sigmund, Steven G. Johnson, "Limits to surface-enhanced Raman scattering near arbitrary-shape scatterers," Proc. SPIE 11462, Plasmonics: Design, Materials, Fabrication, Characterization, and Applications XVIII, 114621R (20 August 2020); doi: 10.1117/12.2567352

SPIE.

Event: SPIE Nanoscience + Engineering, 2020, Online Only

Limits to surface-enhanced Raman scattering near arbitrary-shape scatterers

Mohammed Benzaouia[a], Jérôme Michon[b], Rasmus E. Christiansen[c,d], Wenjie Yao[a], Owen D. Miller[e], Ole Sigmund[c], and Steven G. Johnson[f]

[a]Massachusetts Institute of Technology, Cambridge, MA 02139, USA
[b]Massachusetts Institute of Technology, Cambridge, MA 02139, USA
[c]Technical University of Denmark, Nils Koppels Alle, Building 404, 2800 Kongens Lyngby, Denmark
[d]NanoPhoton—Center for Nanophotonics, Technical University of Denmark, Ørsteds Plads 345A, DK-2800 Kgs. Lyngby, Denmark
[e]Yale University, New Haven, CT 06520, USA
[f]Massachusetts Institute of Technology, Cambridge, MA 02139, USA

ABSTRACT

Various scatterers such as rough surfaces or nanostructures are typically used to enhance the low efficiency of Raman spectroscopy (surface-enhanced Raman scattering). In this work, we find fundamental upper bounds on the Raman enhancement for arbitrary-shaped scatterers, depending only on its material constants and the separation distance from the molecule. According to our metric, silver is optimal in visible wavelengths while aluminum is better in the near-UV region. Our general analytical bound scales as the volume of the scatterer and the inverse sixth power of the distance to the active molecule. For periodic scatterers, a second bound with surface-area scaling is presented. Simple geometries such as spheres and bowties are shown to fall short of the bounds. However, using topology optimization based inverse design, we obtain surprising structures maximizing the Raman enhancement. These optimization results shed light to what extent our bounds are achievable.

Keywords: surface enhanced Raman spectroscopy, upper bounds, topology optimization

1. INTRODUCTION

Surface-enhanced Raman scattering (SERS) is a common method used to enhance the low efficiency of Raman spectroscopy. Active molecules are placed in the vicinity of various scatterers that both concentrate the incoming pump field at the Raman material's location as well as enhance the radiated Stokes signal emitted by the Raman material. Optimized textured surfaces and nanostructures with various shapes have been studied, but no study thus far has looked at the possibility of an upper limit to the enhancement achievable in SERS. In our work, we find fundamental upper bounds on the Raman enhancement for arbitrary-shaped scatterers, depending only on its material constants and the separation distance from the molecule. Our method is based on decomposing the problem into two linear problems: concentration of the incident field on the molecule and a dipole emission at the Raman-shifted frequency. Analytical bounds on the power radiated by a dipole near a scatterer of arbitrary shape were previously reported and are based on optimization under energy-conservation constraints.[1] We apply the same method to the field concentration problem and obtain a final bound on SERS enhancement. According to our metric, silver is optimal in visible wavelengths while aluminum is better in the near-UV region. Our general analytical bound scales as the volume of the scatterer and the inverse sixth power of the distance to the active molecule. Tighter bounds can be computed by simple numerical integration using the free-space Green's function. We also compare the bounds to the actual performance of simple structures (spheres and bowties). Numerical computations show that such geometries fall short of the bounds, suggesting further design opportunities for future improvement. While the bounds can be reached in the quasistatic limit, both the bounds and the actual

Further author information: (Send correspondence to Steven G. Johnson)
Steven G. Johnson: stevenj.mit@gmail.com

Plasmonics: Design, Materials, Fabrication, Characterization, and Applications XVIII,
edited by Din Ping Tsai, Takuo Tanaka, Proc. of SPIE Vol. 11462, 114621R
 · doi: 10.1117/12.2567352

performance increase with the scatterer's volume and further shape optimization is required to get closer to the limits for large scatterers. In the case of periodic structures, a second bound for the concentration problem is obtained using reciprocity. The local field enhancement of the scattering problem can in fact be related to the radiative enhancement of the emission problem as well as the finite incident power per unit cell. The use of the radiative bound for the concentration problem leads to a second SERS bound proportional to the surface area of the unit cell. This area-scaling bound highlights the fact that for a periodic structure, only a fraction of the actual volume of the scatterer is effectively used in the scattering. Comparing the two bounds leads to a tighter limit and suggests an optimal period depending on the volume of the scatterer. For large periods, the volume-scaling bound is limiting because of the reduced interactions between the scatterers of the array, while for smaller periods the performance of the array is limited by the area-scaling bound since the intensity received by each sphere is reduced compared to the non-periodic case. Motivated by the results from the bounds, we also perform freeform shape optimization ("topology optimization", TO) of the total Raman enhancement, and obtain surprising structures $\sim 60\times$ better than optimized coupled-sphere or bowtie. Such results are a proof-of-concept of Raman TO in 2d systems, and the significant enhancements suggest promising results for future improvements in practical 3d Raman sensing.

2. RAMAN BOUNDS

We consider the configuration represented in the inset of Fig. 1-a to describe Raman scattering. An incident "pump" planewave $\mathbf{E_{inc}}$ is scattered by the nanostructure, leading to a near-field enhancement. A Raman-active molecule close to the structure then acquires a dipole moment proportional to the enhanced field, $\mathbf{p} = \boldsymbol{\alpha}_\mathrm{R}\mathbf{E}$ where $\boldsymbol{\alpha}_\mathrm{R}$ is the Hermitian (usually real-symmetric) Raman polarizability tensor. The power radiated by the dipole in the far field at the Raman frequency is our quantity of interest and is given by $P = |\boldsymbol{\alpha}_\mathrm{R}\mathbf{E}|^2 P_\mathbf{p}$ where $P_\mathbf{p}$ is the power radiated by a unit-vector dipole $\hat{\mathbf{p}} = \boldsymbol{\alpha}_\mathrm{R}\mathbf{E}/|\boldsymbol{\alpha}_\mathrm{R}\mathbf{E}|$. If we note P_b the power radiated by a unit-vector dipole in the background medium (in absence of the scatterer), the Raman enhancement can then be defined as:

$$q = \frac{|\boldsymbol{\alpha}_\mathrm{R}\mathbf{E}|^2 P_\mathbf{p}}{\|\boldsymbol{\alpha}_\mathrm{R}\|^2 |\mathbf{E_{inc}}|^2 P_b}, \tag{1}$$

where $\|.\|$ is the induced norm (which gives an upper bound on the magnitude of $\hat{\mathbf{p}}$ for any $\mathbf{E}$ orientation). We see that the enhancement comes from two parts: radiation enhancement ($q_\mathrm{rad} = P_\mathbf{p}/P_b$) and local field (or focusing) enhancement ($q_\mathrm{loc} = |\boldsymbol{\alpha}_\mathrm{R}\mathbf{E}|^2/\|\boldsymbol{\alpha}_\mathrm{R}\|^2|\mathbf{E_{inc}}|^2$).

We can bound the total enhancement by bounding both contributions, as explained in detail in Ref. 2. In particular, if we assume that the tensor $\boldsymbol{\alpha}_\mathrm{R}$ is isotropic and consider that the scatterer is enclosed in a simple structure (such as a half-space or the outside of a sphere) that is separated from the Raman-active molecule by a distance d, we obtain analytical bounds in the limit of *small* d (assuming a free-space background):

$$q \lesssim \frac{3\pi}{2}\beta^2 \frac{V}{k_r^3 d^6} \frac{|\chi_r|^2}{\mathrm{Im}\chi_r} \left(\frac{|\chi_p|^2}{\mathrm{Im}\chi_p}\right)^2, \tag{2}$$

where $\chi(=\epsilon-1)$ is the material susceptibility, V the scatterer volume, k the wavenumber and the subscripts p and r denote the pump and Raman frequencies at which the variables are evaluated. β is a geometrical factor equal to $1/(6\pi)$ for a full sphere, $1/(12\pi)$ for a half-sphere, and $1/(32\pi)$ for a half-plane.[2]

The fundamental limit in Eq. 2 scales as V/d^6. The factor $1/d^6$ is related to both the radiation of the dipole ($1/d^3$) and the coupling to it ($1/d^3$), while the factor V is due to the planewave coupling. In practice, the Raman frequency shift is small enough so that the bounds do not change much when the expressions are simply evaluated at the same (pump or Raman) frequency. In this case, the bound is simply proportional to $\left(|\chi|^2/\mathrm{Im}\chi\right)^3$. This material figure of merit can be used to compare the optimal performance of different materials and is shown in Fig. 1-a. We note that silver (Ag) has the highest bound at visible wavelengths but is outperformed by aluminum (Al) in the near-UV region.

We also simulated two of the most common nanostructures used in SERS: triangular prisms used in a bowtie configuration, and a sphere. Results are shown in Fig. 1-b where we used silver, which is the best-performing

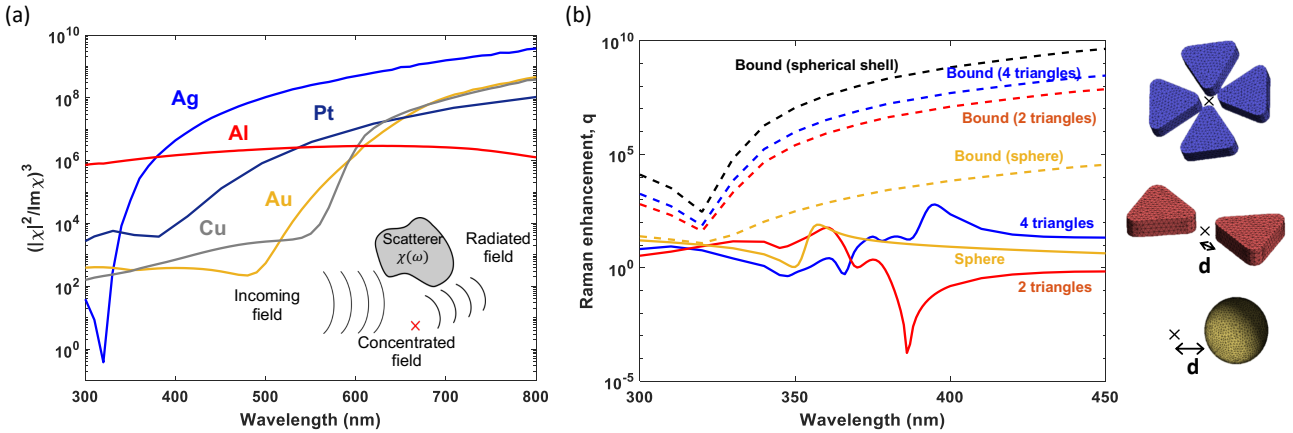

Figure 1. (a) Comparison of the upper bound metric for conventional metals used in SERS. Inset: Illustration of SERS configuration. The pump field is incident onto a scatterer, near which lies the Raman-active molecule. Through the nonlinear Raman process, the molecule behaves as a dipole emitting a Raman-shifted field. The Raman field interacts with the scatterer and is emitted to the far-field. (b) Raman enhancement upper bounds (dashed lines) and actual performances (full lines) for common SERS Ag structures. The distance to the emitter is $d = 20$ nm for all structures. The sphere has a radius of 10 nm. The triangles have a side of 160 nm, height of 30 nm, and tip curvature of 16 nm. The incident field's polarization is aligned with the sphere-emitter and triangle-emitter direction. Black dashed line represents analytic shape-independent bound for structures that lie inside a spherical shell around the Raman molecule. Coloured dashed lines represent shape-dependent bounds for each specific structure.

Raman material at visible frequencies and which also satisfies the resonance condition for χ, unlike e.g. gold. The geometry of the triangles was taken from Ref. 3. We plotted both the shape-independent bound ($\sim$ Eq.2) by considering the exterior of a spherical shell and using the largest volume of all scatterers (4-triangle bowtie), as well as a shape-dependent bound for each structure (given in Ref. 2). Results in Fig. 1-b show that all structures fall short of the shape-independent bound by several orders of magnitude. The performances of bowties also lie far from their shape-specific limits. Only the sphere approaches its bound, at frequencies greater than the plasma frequency of silver.

Using reciprocity, we also found a second bound in the case of periodic structures, as shown in Ref. 2. This new bound is now proportional to $\left(|\chi|^2/\mathrm{Im}\chi\right)^2$ (rather than $\left(|\chi|^2/\mathrm{Im}\chi\right)^3$) and scales as the surface area of the unit cell instead of the volume of the scatterer. This area-scaling bound highlights the fact that for a periodic structure, only a fraction of the actual volume of the scatterer (proportional to the unit-cell area) is effectively "used" in the scattering. Combining the volume-scaling and area-scaling bounds leads to a tighter bound with different behavior as a function of the period. Overall, maximum enhancement due to periodicity occurs at the smallest possible period, where increased interactions between the scatterers dominate the decrease in incident intensity received by each unit cell.[2]

3. TOPOLOGY OPTIMIZATION

Encouraged by results from bounds, we also performed freeform shape optimization ("topology optimization", TO) to maximize Raman enhancement as discussed in details in Ref. 4. The Raman scattering process is modeled as described in the previous section using two sequentially-coupled frequency-domain electromagnetic simulations. In particular, the system is first excited by an incident planewave at the pump frequency. Afterwards, the Raman molecule is modeled as a dipole source at the Raman-shifted frequency (with dipole moment given by the polarizability tensor $\boldsymbol{\alpha}_{\mathrm{R}}$ multiplied by the electric field obtained in the first simulation) which then allows to compute the total emitted power. Simulations are for two-dimensional (2d) structures with in-plane polarization (Fig 2-a).

The use of density-based topology optimization operates by introducing a continuous design field to control the physical material distribution, enabling the use of adjoint sensitivity analysis and gradient-based optimization

algorithms to efficiently solve design problems with potentially billions of design degrees of freedom. Hence, the approach provides near-unlimited design freedom, with a computational complexity dominated by the solution of the Maxwell equations, utilizing mature finite-element techniques.[4]

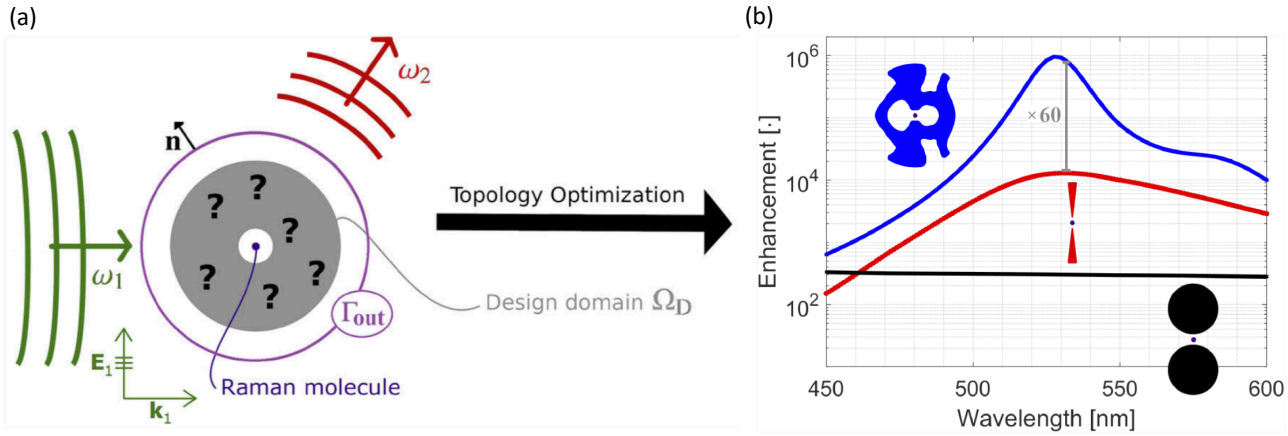

Figure 2. (a) A sketch of the Raman scattering design problem where a Raman molecule (blue) in air background is surrounded by the design domain Ω_D (gray) and excited by an incident planewave (green). Optimization maximizes the total emitted power (red) through Γ_{out}. Distance separating the molecule and the structure is fixed at 10 nm. The outside radius of the optimization domain Ω_D is fixed at 100 nm. Results presented here assume a zero Raman frequency shift. (b) Raman enhancement as a function of wavelength, for a molecule placed at the center of different silver nanostructures (dark blue dot) relative to a molecule placed in free space. A topology-optimized structure (blue), a bowtie antenna (red) and coupled-cylinder antenna (black) are considered, all designed to maximize enhancement at 532 nm.

Solutions are presented in Fig 2-b, where topology optimization results are also compared to reference geometries (coupled triangles and discs). Reference structures are parameter-optimized (through the radius of the discs and through the tip-angle and the side length of the triangles) to maximize performance at the targeted wavelength (532 nm). We see that topology optimization leads to a surprising structure that fully encloses the molecule and that, in some sense, is a fusion of different features tailored to enhance either focusing or emission.[4] The TO structure has a maximum enhancement of $\approx 8 \cdot 10^5$, which is $60\times$ larger than bowtie-antenna enhancement ($\approx 1.3 \cdot 10^5$) and $2.6 \cdot 10^3\times$ larger than coupled-discs enhancement ($\approx 3 \cdot 10^2$). These extreme enhancement results, serve as a proof-of-concept suggesting promising improvements for practical 3d structures.

Topology optimization has also been used to optimize focusing and radiation enhancements separately, showing the need to optimize both processes simultaneously.[4] When compared to the fundamental upper bounds presented in section 2, we find that the TO structure (optimized for radiation) comes to within a factor of 4 of the radiation bound. This is a reasonable difference that can be attributed to the length-scale imposed during optimization as well as simplifications leading to the bound. On the other hand, the TO structure optimized for focusing is $\sim 6 \cdot 10^2$ smaller than the bound. This suggests that the upper limit may not be tight, in the sense that it may be difficult to achieve optimal coupling to both far-field and near-field, as is required by the focusing bound. The discrepancy may also be due to the fact that the outside radius of the domain Ω_D was fixed in the optimization. The focusing bound rather suggests the need of a large volume for a good coupling to the planewave. This can for example be seen in the area-scaling bound for periodic structures where we obtained a $\left(|\chi|^2/\mathrm{Im}\chi\right)^2$ dependence due to the *finite* incident power per unit cell. A similar dependence on the material metric has indeed been noticed in optimized structures.[4] In general, it remains an open problem, for future theoretical and numerical investigations, to understand practical limitations related to the near-field focusing problem.

4. CONCLUSION

We presented general analytical upper bounds that can be used for an easy estimation of the optimal performance of SERS. Results show a large range for potential improvement compared to typical structures. In particular, we obtained very promising results using topology optimization of 2d structures with substantial enhancement compared to parameter-optimized simple structures.

FUNDING

National Science Foundation (1453218, 1709212); Air Force Office of Scientific Research (FA9550-17-1-0093); Army Research Office (W911NF-13-D-0001); the Danish National Research Foundation through NanoPhoton Center for Nanophotonics (grant no. DNRF147).

REFERENCES

[1] Miller, O. D., Polimeridis, A. G., Reid, M. T. H., Hsu, C. W., DeLacy, B. G., Joannopoulos, J. D., Soljačić, M., and Johnson, S. G., "Fundamental limits to optical response in absorptive systems," *Optics Express* **24**, 3329–3364 (feb 2016).

[2] Michon, J., Benzaouia, M., Yao, W., Miller, O. D., and Johnson, S. G., "Limits to surface-enhanced Raman scattering near arbitrary-shape scatterers," *Optics Express* **27**(24), 35189–35202 (2019).

[3] Kaniber, M., Schraml, K., Regler, A., Bartl, J., Glashagen, G., Flassig, F., Wierzbowski, J., and Finley, J. J., "Surface plasmon resonance spectroscopy of single bowtie nano-antennas using a differential reflectivity method," *Scientific Reports* **6**, 23203 (mar 2016).

[4] Christiansen, R. E., Michon, J., Benzaouia, M., Sigmund, O., and Johnson, S. G., "Inverse design of nanoparticles for enhanced Raman scattering," *Optics Express* **28**(4), 4444–4462 (2020).